Journal of Microscopy, Vol. 229, Pt 2 2008, pp. 197–202
Received 29 September 2006; accepted 6 March 2007

Broadband optical near-field microscope for nanoscale absorption spectroscopy of organic materials

R. POMRAENKE*, C. ROPERS*, J. RENARD*, C. LIENAU*†,
L. LÜER‡, D. POLLI‡ & G. CERULLO‡
**Max-Born-Institut für Nichtlineare Optik und Kurzzeitspektroskopie, 12489 Berlin, Germany*
†Institut für Physik, Carl von Ossietzky Universität Oldenburg, 26111 Oldenburg, Germany
‡ULTRAS-CNR-INFM, Dipartimento di Fisica, Politecnico di Milano, Piazza Leonardo da Vinci 32, I-20133 Milano, Italy

Key words. Near-field microscopy, optical spectroscopy, polymer nanostructures.

Summary

Conjugated organic materials in the solid state are generally amorphous or polycrystalline, with local order only achieved in mesoscopic domains with size ranging from a few tens to a few hundreds of nanometres. Understanding the interplay between mesoscopic order and macroscopic behaviour of these materials calls for a spatially resolved study of their optical properties. Near-field scanning optical microscopy allows one in principle to beat the diffraction limit in optical imaging. A quantitative measurement of nanoscale absorption spectra is, however, complicated by the difficulty of obtaining broadband near-field illumination with sufficiently high intensity. Here we demonstrate a near-field spectrometer with 100-nm spatial resolution based on an ultrabroadband Ti:sapphire oscillator coupled to an aperture-based near-field scanning optical microscopy, enabling structural phase-selective imaging of organic materials at the nanoscale. In polycrystalline phtalocyanine films we can distinguish between the crystalline and the amorphous phase, thus providing previously unavailable information on their mesoscopic texture.

Introduction

Conjugated organic materials exhibit a unique combination of characteristics: the electronic and optical properties of semiconductors are linked with the processing advantages and mechanical properties of plastics (Friend *et al.*, 1999). These materials, also known as 'organic semiconductors', have given rise to the field of 'plastic electronics', with devices such as light-emitting diodes, lasers, photovoltaic cells, field-effect transistors and all-organic integrated circuits (Forrest, 2004). One of the peculiar features of organic semiconductors, as compared to inorganic ones, is their structural inhomogeneity. It is very difficult to grow single crystals of size and optical quality good enough for applications; in fact these materials, in the solid state, are generally amorphous or polycrystalline, with local order only achieved in mesoscopic domains with size ranging from a few tens to a few hundreds of nanometres (Nguyen *et al.*, 2000; Schwartz, 2003). In addition, in many devices blends of different molecules are often used, which, owing to the low entropy of mixing, undergo phase separation into domains of varying size and shape (Halls *et al.*, 1995). Many studies have proven that the size and type of the mesoscopic structures has a decisive influence on fluorescence quantum yield, charge carrier mobility and generation efficiency, parameters that must be fine tuned against each other to optimize each kind of optoelectronic application (Sirringhaus *et al.*, 1999). A particularly crucial aspect is the morphology at grain boundaries, e.g. at the electrode/organic interface or in a bulk heterostructure (Morteani *et al.*, 2004; Loi *et al.*, 2006). Therefore, the optimization of organic device technology calls for an imaging method offering morphology contrast on the nanoscale. Atomic force microscopy can distinguish domains of different heights, but cannot unambiguously assign them to different phases/molecular species owing to its lack of chemical sensitivity.

Optical spectroscopies, on the other hand, are powerful tools to resolve morphological changes because of the effects of the morphology on the local fluorescence/absorption spectra, but in their traditional implementations their spatial resolution is limited by diffraction to dimensions of the order of the wavelength. The near-field scanning optical microscope (NSOM) allows one to overcome the diffraction limit by confining the light on the nanometre scale using a

Correspondence to: C. Lienau. Tel: +49 441 798 3485; fax: +49 441 798 3890; e-mail: christoph.lienau@uni-oldenburg.de

suitable probe. In the so-called aperture NSOM, a nanometre-sized aperture, usually realized by a metal-coated tapered optical fibre, confines the optical field in an evanescent, nonpropagating wave. The latter can be transformed into a propagating wave by interaction with a sample approached to the aperture at a distance much smaller than the wavelength, i.e., in the optical near field. An NSOM image is acquired by raster scanning the probe across the sample and is accompanied by a high-resolution topographic map. The typical spatial resolution of the aperture NSOM is ≈100 nm.

The NSOM technique has been applied to the characterization of thin organic films (DeAro *et al.*, 1997; Stevenson *et al.*, 2001; Teetsov & Vanden Bout, 2001; Chappell *et al.*, 2003; Cadby *et al.*, 2005), to correlate the optical properties with sample morphology and to study the composition of phase separated polymer blends. In these experiments, the NSOM is illuminated by a single laser wavelength and the light transmitted/reflected by the sample or its photoexcited fluorescence is collected by the detector. In special cases, this allows for a clear interpretation by imaging prominent fluorescence wavelengths of known pure phases (Stevenson *et al.*, 2001; Chappell *et al.*, 2003; Cadby *et al.*, 2005). More generally, however, an unambiguous assignment of morphological phases requires the measurement of nanoscale absorption spectra, because the shape of optical absorption bands is strongly influenced by intermolecular interactions. Such measurements turned out to be experimentally highly challenging, partly because of the difficulty in generating broadband near-field illumination with sufficiently high intensity. Broadband emission spectra can be readily obtained from incoherent light sources (such as an arc lamp) (Seidel *et al.*, 2001), but these can be coupled only with very poor efficiency to the NSOM optical fibre. On the other hand, femtosecond lasers provide spatially coherent ultrabroadband light beams either directly from the laser oscillator or by supercontinuum generation, and such high-quality beams can be efficiently coupled into the NSOM probe (Mikhailovsky *et al.*, 2003, 2004; Nagahara *et al.*, 2004).

In this paper, we report on a broadband near-field spectrometer based on a an aperture NSOM coupled to a few-optical-cycle Ti:sapphire laser. The system enables us to measure nanoscale absorption spectra over the 650–950-nm wavelength range with sub-100-nm spatial resolution. We apply this novel instrument to the study of organic semiconductor thin films and are able to access previously unavailable information on their nanoscale morphologic texture. In particular, we study films of oxotitanyl phthalocyanine (TiOPc), which is among the most promising candidates for organic bulk heterojunction photovoltaics. The supramolecular arrangement in such films can be in either amorphous or polycrystalline phases, which show drastically different absorption spectra. Our instrument enables us to spatially resolve the distribution of these phases within the film, providing important information for optimization of photovoltaic devices.

Materials and methods

TiOPc samples

Depending on preparation conditions, TiOPc films consist of either amorphous or crystalline phases; among the latter, phases II and Y show good hole conduction, high photostability, strong optical absorption from the red to near-infrared spectral region and very efficient charge separation (Saito *et al.*, 1993; Yamashita *et al.*, 1993, 1994). After vapour deposition at room temperature, TiOPc films are in the amorphous phase; they can, however, be partially or totally converted to the crystalline phase II by either thermal annealing (Yamashita *et al.*, 1994) or vapour treatment with ethanol or tethrahydrofurane (THF, Saito *et al.*, 1993; Del Caño *et al.*, 2005). The spatial distribution of different phases in a film determines to a large extent its conductive properties and is of paramount importance for applications.

TiOPc samples were prepared on glass slides by vapour deposition in high vacuum (base pressure 10^{-6} mbar) at an evaporation rate of about 2 Å/s to a thickness of ≈70 nm. Pristine films were in the amorphous phase. Subsequent vapour treatment was performed in THF-saturated air at room temperature under simultaneous monitoring of the absorption spectrum. The growth of the crystalline phase II band started ≈2 min after the beginning of the treatment; conversion reached its stationary state after ≈20 min. By interrupting the process at different times, we could obtain films with different degrees of conversion.

Broadband NSOM

The experimental setup of the home-built NSOM operating at room temperature inside a vacuum chamber is shown in Fig. 1. For these experiments, the vacuum chamber is used to shield the microscope from air turbulence; the measurements were done at room temperature and atmospheric pressure. The microscope operates on an optical table to avoid any disturbances from floor oscillations. Illumination is provided by an ultrabroadband Ti:sapphire oscillator (Femtolaser model Femtosource Rainbow, Vienna, Austria) generating 6-fs pulses with a spectrum ranging from 650 to 970 nm (see a typical laser spectrum in Fig. 1). Only a 3-mW portion of the laser output is coupled to an Al-coated tapered optical fibre with a 50–100-nm aperture to prevent melting the tip; the aperture size of the fibres was determined by independent calibration measurements before and after the actual measurements and showed no degradation during the course of the experiment. The fibre tip is glued on a commercial quartz tuning fork, which is used as a detector for shear-force tip-sample distance regulation in combination with a 4-μm piezoelectric

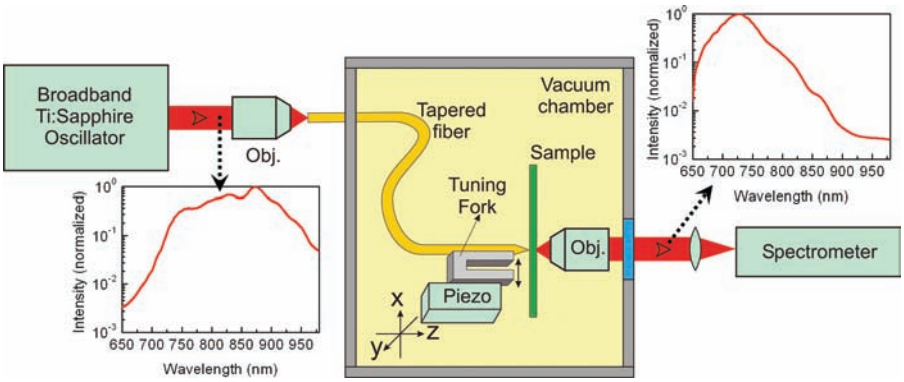

Fig. 1. Experimental setup of the broadband NSOM, with spectra generated by the Ti:sapphire oscillator and transmitted through the tip. Obj, microscope objective.

transducer and an electronic feedback loop; a constant tip-sample distance of 10 nm is maintained during scanning. The tuning fork is excited at its resonance frequency around 32 kHz and oscillates with an amplitude of less than 5 nm. The tip-setup is mounted on a linearized piezoelectric translation stage (Physik Instrumente P730.20, Karlsruhe, Germany) allowing x-y scans with a range up to 100×100 μm. The piezoelectric translation stage (with mounted tuning fork and tip) is located in a combination of three motorized translation stages for coarse positioning and approach. The transmitted light is collected by a 0.4-NA-long working distance microscope objective and imaged on the entrance slit of a spectrometer (Acton Spectra Pro 500i, Acton, MA, USA) equipped with a high-sensitivity liquid-nitrogen-cooled CCD detector, thus enabling simultaneous measurement, for a given sample position, of the absorption at all wavelengths covered by the laser spectrum. By raster scanning the sample under the tip, it is then possible to record the transmitted light spectrum at every sample position, $I_T^{\text{sample}}(\omega, x, y)$. Local absorption spectra are obtained by comparing $I_T^{\text{sample}}(\omega, x, y)$ with the spectrum of the light, $I_T^{\text{glass}}(\omega)$, transmitted through a transparent glass substrate and held at a fixed distance of 10 nm from the near-field fibre probe and by computing the absorbance:

$$A(\omega, x, y) = -\log\left(\frac{I_T^{\text{sample}}(\omega, x, y)}{I_T^{\text{glass}}(\omega)}\right).$$

We found it important to record complete absorption spectra at each sample position, rather than sequentially acquiring images at different wavelengths, to speed up the measurement, thus avoiding drifts in the experimental setup as well as tip-induced morphological changes of the sample, particularly critical with organic soft matter. A typical transmitted light spectrum, for an integration time of 50 ms, is shown in Fig. 1: we achieve a count rate well above the dark current background for the entire 670–950-nm wavelength range, allowing fast scans (10–15 min for a complete image) with high signal-to-noise ratio.

Results and discussion

Figure 2 shows as a black line the far-field absorption spectrum of an untreated TiOPc film prepared by vapour deposition. It is characteristic for the amorphous phase and consists of a broad Soret band centred at 343 nm (not displayed) and a Q band peaking at 720 nm, with a well-defined vibronic replica at 653 nm. Figure 2 also displays (red line) the absorption spectra of TiOPc after prolonged vapour treatment (43 min) with THF; the formation of the crystalline phase II is evidenced by the development of a red-shifted absorption band, peaking at 830 nm, and the corresponding reduction of the peak of the amorphous phase at 720 nm. The 830-nm peak has been attributed either to excitonic delocalization induced by the

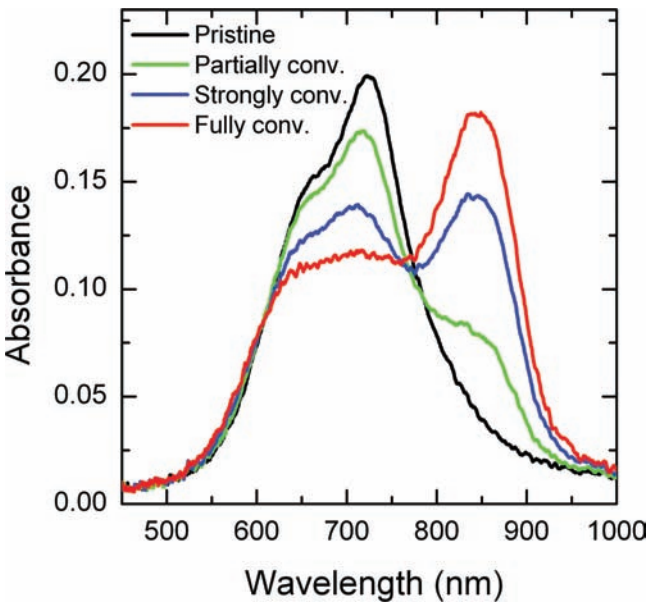

Fig. 2. Far-field absorption spectra of TiOPc thin films as deposited and after varying exposure times to THF atmosphere. The development of the crystalline phase is evidenced by the growth of the absorption band at 830 nm.

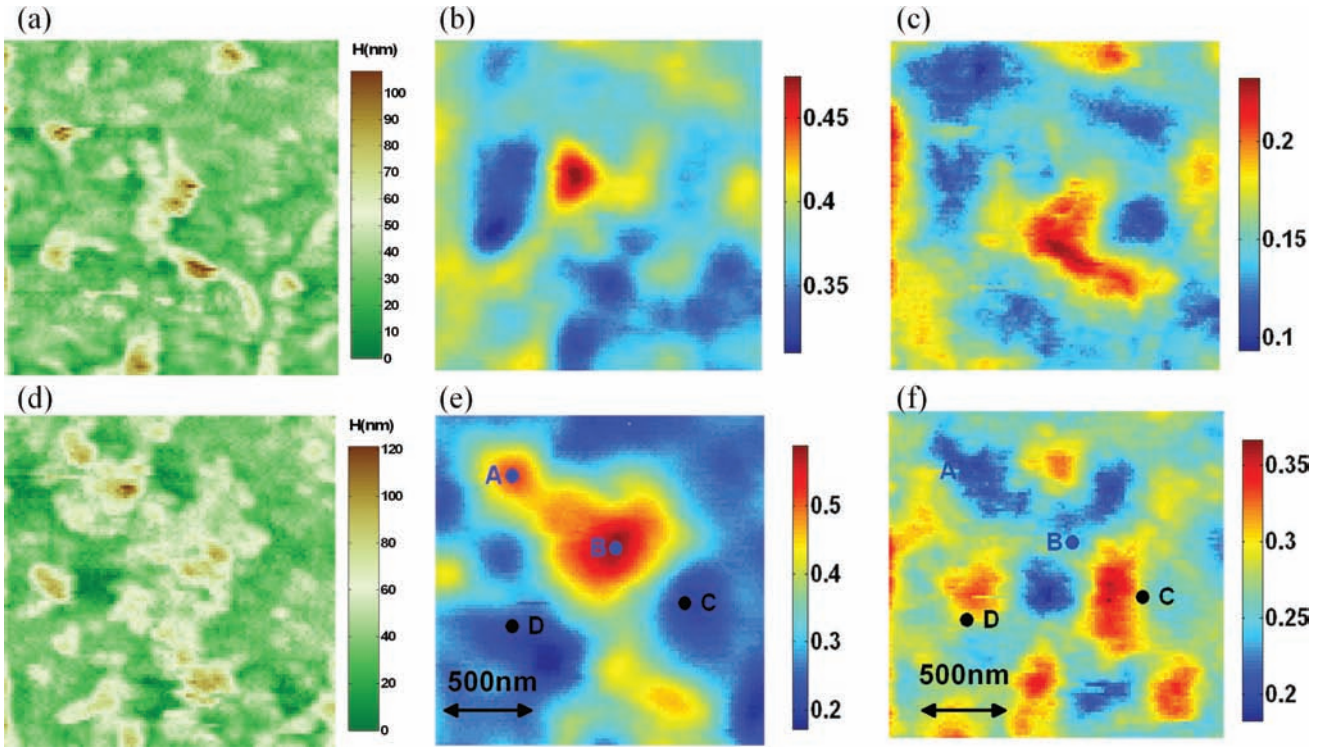

Fig. 3. Topography (a, d) and absorption maps in the 700–750 nm (b, e) and 820–900 nm (c, f) wavelength ranges. Top row: partially converted sample; bottom row: strongly converted sample. The corresponding far-field spectra are shown in Fig. 2, green and blue lines, respectively. At points A–D, local absorption spectra are displayed in Fig. 4.

formation of *J* aggregates in the crystalline phase (Yamashita *et al.*, 1994) or to molecular distortion lifting the degeneracy of the fundamental electronic transition (Mizuguchi *et al.*, 1995). The formation of the crystalline phase II can be interrupted at any time by removing the vapour, resulting in partially converted films with a stable phase composition. Figure 2 shows absorption spectra corresponding to a partially converted film (5 min, green line) and a strongly converted one (7 min, blue line).

We first studied with the broadband NSOM the slightly converted film. Figure 3 shows absorbance maps in two different wavelength regions: 700–750 nm (b) and 820–900 nm (c), corresponding to the absorption peaks of the amorphous and crystalline phase, respectively. For comparison, the topographic map is given in Fig. 3(a). One clearly sees strong absorbance variations on a sub-micrometre length scale, which are not correlated in the two maps: in fact, some areas with higher absorption around 725 nm (corresponding to the peak of the amorphous phase) show less absorption around 830 nm (corresponding to the peak of the crystalline phase) and vice versa. In addition, there is no correlation between the topographic and absorption maps. The same considerations hold for the strongly converted film, of which we show absorbance maps for the 700–750 nm range (e) and the 820–900 nm range (f) together with the topographic map (d).

The absence of a clear correlation between absorption images and topography excludes the presence of topographic artefacts (Hecht *et al.*, 1997); therefore, Figs 3(b, c, e and f) represent images of locally resolved optical absorption. However, even in the absence of artefacts, Lambert-Beer's law still requires a correlation between optical absorption and the path length of the transmitted light and hence the topography. The fact that this correlation cannot be observed, already points to compositional inhomogeneity of the films, superposing the effect of path length variation. This is confirmed by the presence of anti-correlations between the two wavelength ranges for the amorphous and the crystalline state, respectively. In a sample with a homogeneous contribution of the crystalline phase, the images (Figs 3b and c, and also Figs 3e and f) should be strictly correlated throughout space. However, we can find regions where a high absorption of the crystalline phase corresponds to a low absorption of the amorphous phase (see points C and D). In other regions, the amorphous phase absorbs more strongly than the crystalline phase (points A and B). These local anti-correlations are therefore evidence of strong spatial fluctuations in the local composition of the sample resulting from pronounced structural phase disorder in the film.

Figure 4 shows measured near-field absorption spectra at four representative positions within the scan (indicated by dots in Fig. 3). The local spectra show similar features as the far-field

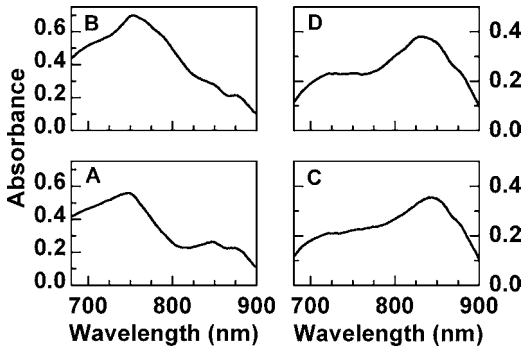

Fig. 4. Near-field absorption spectra at selected positions on the sample, corresponding to the points marked in Fig. 3.

ones, in particular, the absorption peaks for the amorphous and the crystalline phase are clearly observed. The slight red shift (15–20 nm) in the near-field spectra with respect to the far-field ones (see Fig. 2) for the amorphous phase can be explained by a phase shift between the incident electromagnetic field and the field re-emitted by the polymer nanostructures (Mikhailovsky *et al.*, 2003, 2004). In a quantitative study, which will be reported elsewhere, we managed to reproduce this shift by introducing a $\approx$0.1 rad phase shift for the amorphous phase. The local spectra show dramatic changes with position, ranging from a nearly amorphous structure (positions A and B) to a nearly completely converted one (positions C and D). In the investigated samples, such fluctuations are resolved on a scale of about 100 nm. This demonstrates the ability of the broadband NSOM to microscopically resolve phase disorder and to differentiate among structural phases in our sample with 100-nm spatial resolution. It is interesting to note that the far-field spectrum of the sampled region, given in Fig. 2, blue line, qualitatively resembles the average of the spectra displayed in Fig. 4 for the strongly converted sample. This exemplifies the additional information that can be obtained by local absorption imaging: contrary to what one might expect from the far-field spectra, there are large regions of the amorphous phase interfacing the crystalline regions. This has strong consequences on the optoelectronic properties like, charge mobility and charge separation efficiency. The broadband NSOM provides a tool to optimize deposition parameters of these materials by monitoring their microscopic morphology.

In conclusion, we have demonstrated a broadband near-field spectrometer with 100-nm spatial resolution, which allows for structural phase-selective imaging of organic materials at the nanoscale. Spatially selective nanoscale phase transformations of organic solids by vapour treatment are directly evidenced. We believe that this instrument can allow new insight into the mesoscopic structure of organic materials by providing information not available with other techniques. The wavelength range of the spectrometer can be further extended both in the short-wavelength range (blue/green part of the visible spectrum and near-UV) and the near-IR by supercontinuum generation in a microstructured fibre (Russel, 2003). In addition, by using a scattering NSOM approach (Hillenbrand & Keilmann, 2002), we envision an order of magnitude improvement in spatial resolution of absorption spectra, down to the 10-nm feature size characteristic of excitons in organic materials. In this way, we will be able to study the phase composition at heterostructure interfaces, of paramount importance for optimization of both emissive and photovoltaic devices (Tsuzuki *et al.*, 2000; Peumans *et al.*, 2003; Diamant & Zaban, 2004), in the most direct way by optical imaging.

Acknowledgement

The authors acknowledge support from the European Community-Access to Research Infrastructure Action of the Improving Human Potential Program, Contract RII3-CT-2003-506350, from the Italian FIRB project 'Nanotechnologies and Nanodevices for the Information Society' and from the Deutsche Forschungsgemeinschaft via the Sonderforschungsbereich SFB 296.

References

Cadby, A., Dean, R., Fox, A.M., Jones, R.A.L. & Lidzey, D.G. (2005) Mapping the fluorescence decay lifetime of a conjugated polymer in a phase-separated blend using a scanning near-field optical microscope. *Nano. Lett.* **5**, 2232–2237.

Chappell, J., Lidzey, D.G., Jukes, P.C., *et al.* (2003) Correlating structure with fluorescence emission in phase-separated conjugated polymer blends. *Nat. Mater.* **9**, 616–621.

DeAro, J.A., Weston, K.D., Buratto, S.K. & Lemmer, U. (1997) Mesoscale optical properties of conjugated polymers probed by near-field scanning optical microscopy. *Chem. Phys. Lett.* **277**, 532–538.

Del Caño, T., Parra, V., Rodríguez-Méndez, M.L., Aroca, R.F. & De Saja, J.A. (2005) Characterization of evaporated trivalent and tetravalent phthalocyanines thin films: Different degree of organization. *Appl. Surf. Sci.* **246**, 327–333.

Diamant, Y. & Zaban, A. (2004) A high surface area organic solar cell prepared by electrochemical deposition. *J. Sol. Energ. Eng.* **126**, 893–897.

Friend, R.H., Gymer, R.W., Holmes, A.B., *et al.* (1999) Electroluminescence in conjugated polymers. *Nature* **397**, 121–128.

Forrest, S.R. (2004) The path to ubiquitous and low-cost organic electronic appliances on plastic. *Nature* **428**, 911–918.

Halls, J.J.M., Walsh, C.A., Greenham, N.C., Marseglia, E.A., Friend, R.H., Moratti, S.C. & Holmes, A.B. (1995) Efficient photodiodes from interpenetrating polymer networks. *Nature* **376**, 498–500.

Hecht, B., Bielefeldt, H., Inouye, Y., Pohl, D.W. & Novotny, L. (1997) Facts and artifacts in near-field optical microscopy. J. *Appl. Phys.* **81**, 2492–2498.

Hillenbrand, R. & Keilmann, F. (2002) Material-specific mapping of metal/semiconductor/dielectric nanosystems at 10 nm resolution by backscattering near-field optical microscopy. *Appl. Phys. Lett.* **80**, 25–27.

Loi, M.A., Rost-Bietsch, C., Murgia, M., Karg, S., Riess, W. & Muccini, M. (2006) Tuning optoelectronic properties of ambipolar organic light-emitting transistors using a bulk-heterojunction approach. *Adv. Funct. Mat.* **16**, 41–47.

Mikhailovsky, A.A., Petruska, M.A., Stockman, M.I. & Klimov, V.I. (2003) Broadband near-field interference spectroscopy of metal nanoparticles using a femtosecond white-light continuum. *Opt. Lett.* **28**, 1686–1688.

Mikhailovsky, A.A., Petruska, M.A., Li, K., Stockman, M.I. & Klimov, V.I. (2004) Phase-sensitive spectroscopy of surface plasmons in individual metal nanostructures. *Phys. Rev. B* **69**, 085401–085406.

Mizuguchi, J. , Rihs, G. & Karfunkel, H.R. (1995) Solid-state spectra of titanylphthalocyanine as viewed from molecular distortion. *J. Phys. Chem.* **99**, 16217–16227.

Morteani, A.C., Sreearunothai, P., Herz, L.M., Friend, R.H. & Silva, C. (2004) Exciton regeneration at polymeric semiconductor heterojunctions. *Phys. Rev. Lett.* **92**(247402), 1–4.

Nagahara, T., Imura, K. & Okamoto, H. (2004). Time-resolved scanning near-field optical microscopy with supercontinuum light pulses generated in microstructure fiber. *Rev. Sci. Instrum.* **75**, 4528–4533.

Nguyen, T.-Q., Martini, I.B., Liu, J. & Schwartz, B.J. (2000) Controlling interchain interactions in conjugated polymers: The effects of chain morphology on exciton-exciton annihilation and aggregation in MEH-PPV films. *J. Phys. Chem. B* **104**, 237–255.

Peumans, P., Uchida, S. & Forrest, S.R. (2003) Efficient bulk heterojunction photovoltaic cells using small-molecular-weight organic thin films. *Nature* **425**, 158–162.

Russel, P. (2003) Photonic crystal fibers. *Science* **299**, 358–362.

Saito, T., Sisk, W., Kobayashi, T., Suzuki, S. & Iwayanagi, T. (1993) Photocarrier generation processes of phthalocyanines studied by photocurrent and electroabsorption measurements. *J. Phys. Chem.* **97**, 8026–8031.

Schwartz, B.J. (2003) Conjugated polymers as molecular materials: How chain conformation and film morphology influence energy transfer and interchain interactions. *Annu. Rev. Phys. Chem.* **54**, 141–172.

Seidel, J., Grafström, S., Loppacher, Ch., Trogisch, S., Schlaphof, F. & Eng, L.M. (2001) Near-field spectroscopy with white-light illumination. *Appl. Phys. Lett.* **79**, 2291–2293.

Sirringhaus, H., Brown, P.J., Friend, R.H., *et al.* (1999) Two-dimensional charge transport in self-organized, high-mobility conjugated polymers. *Nature* **401**, 695–688.

Stevenson, R., Riehn, R., Milner, R.G., *et al.* (2001) Ultraviolet-visible near-field microscopy of phase-separated blends of polyfluorene-based conjugated semiconductors. *Appl. Phys. Lett.* **79**, 833–835.

Teetsov, J. & Vanden Bout, D.A. (2001) Imaging molecular and nanoscale order in conjugated polymer thin films with near-field scanning optical microscopy. *J. Am. Chem. Soc.* **123**, 3605–3606.

Tsuzuki, T., Shirota, Y., Rostalski, J. & Meissner, D. (2000) The effect of fullerene doping on photoelectric conversion using titanyl phthalocyanine and a perylene pigment. *Sol. Energ. Mat. Sol. Cells* **61**, 1–8.

Yamashita, A., Maruno, T. & Hayashi, T. (1993) Absorption spectra of organic-molecular-beam-deposited vanadyl- and tytanylphtalocyanine. *J. Phys. Chem.* **97**, 4567–4569.

Yamashita, A., Maruno, T. & Hayashi, T. (1994) Phase-selective formation of titanylphthalocyanine thin films by organic molecular beam deposition. *J. Phys. Chem.* **98**, 12695–12701.